Nuclear Science and Techniques (2025) 36:25
https://doi.org/10.1007/s41365-024-01630-y

Ultra-high quality factor and ultra-high accelerating gradient achievements in a 1.3 GHz continuous wave cryomodule

Jin-Fang Chen[1] · Yue Zong[1] · Xiao-Yun Pu[1] · Sheng-Wang Xiang[1] · Shuai Xing[1] · Zheng Li[1] · Xu-Ming Liu[1] · Yan-Fei Zhai[1] · Xiao-Wei Wu[2] · Yong-Zhou He[1] · Ling-Ling Gong[1] · Ji-Dong Zhang[1] · Shan-Shan Cao[1] · Wen-Ding Fang[1] · Bin-Tuan Zhang[1] · Kai Xu[1] · Yi-Bo Yu[1] · Guang-Hua Chen[1] · Li-Jun Lu[1] · Ya-Wei Huang[3] · Shen-Jie Zhao[1] · Hong-Tao Hou[1] · Zhen-Yu Ma[1] · Ye-Liang Zhao[1] · Xiang Zheng[1] · Jiu-Ce Sun[3] · Sen Sun[1] · Zhi-Qiang Jiang[1] · Yu-Bin Zhao[1] · Meng Zhang[1] · Ying-Bing Yan[1] · Yi-Yong Liu[1] · Qiang Gu[1] · Bo Liu[1] · Li-Xin Yin[1] · Dong Wang[1] · Hai-Xiao Deng[1] · Zhen-Tang Zhao[1]

Received: 25 November 2024 / Revised: 7 December 2024 / Accepted: 8 December 2024 / Published online: 10 January 2025

Abstract
We report the world-leading performance of a 1.3 GHz cryomodule equipped with eight 9-cell superconducting radio-frequency cavities that underwent a medium-temperature furnace baking process. During continuous wave horizontal testing, these cavities achieved unprecedented average intrinsic quality factors of 4.0×10^{10} at 20 MV/m and 3.2×10^{10} at 29 MV/m, with no instances of field emission. The cryomodule demonstrates near-complete preservation of ultra-high quality factors and ultra-high accelerating gradients from vertical to horizontal testing, marking a significant milestone in continuous-wave superconducting radio-frequency accelerator technology. This letter presents the cryomodule development experience, including cavity preparation, cryomodule assembly, degaussing, fast cooldown, and performance testing.

Keywords SRF cryomodule · Mid-T baking · High quality factor · High accelerating gradient

1 Introduction

High Q_0 (quality factor) cryomodules equipped with superconducting radio-frequency (SRF) cavities are key components of modern accelerators, such as high-repetition X-ray FEL facilities [1], high-power extreme ultraviolet lithography light sources [2], and other future high-duty factor colliders [3]. At the Shanghai High Repetition Rate XFEL and Extreme Light Facility (SHINE) [4], more than 50 high Q_0 cryomodules operating in 1.3 GHz continuous-wave (CW) mode will be installed to generate an 8 GeV electron beam. In contrast, extreme ultraviolet lithography light sources require approximately 10 high Q_0 cryomodules operating in 1.3 GHz CW mode for a 1 GeV energy recovery linac. Generally, a high Q_0 cryomodule includes eight 9-cell TESLA cavities [5], eight fundamental power couplers (FPC), one superconducting quadrupole magnet package, and one cold beam-position monitor. The design and advancements of 1.3 GHz cryomodules are primarily attributed to the R&D efforts undertaken in large-scale facilities like the TESLA Test Facility [6], the European XFEL [7], the Linac Coherent Light Source II (LCLS-II) [8], LCLS-II HE [9] and SHINE.

Currently, nitrogen doping (N-doping) [10–14] and medium-temperature (mid-T) baking [15–17] are the two main methods used to enhance the Q_0 values of SRF cavities made of high-purity niobium. N-doping incorporates nitrogen atoms as interstitial impurities into the niobium lattice, lowering the mean free path of the RF penetration layer of niobium, hence the BCS resistance, and reducing the residual resistance [18]. Fermilab and Jefferson Lab

This work was supported by Zhangjiang Laboratory, the SHINE R&D project (No. 2017SHZDZX02), the SHINE project, and the National Natural Science Foundation of China (No. 12125508).

✉ Hai-Xiao Deng
denghx@sari.ac.cn

1 Shanghai Advanced Research Institute, Chinese Academy of Sciences, Shanghai 201204, China

2 Zhangjiang Laboratory, 201210 Shanghai, China

3 ShanghaiTech University, Shanghai 201210, China

developed cryomodules equipped with SRF cavities treated by 2/6 N-doping recipes for LCLS-II [19, 20]. In 2023, 35 cryomodules with 2/6 N-doped cavities were commissioned for the LCLS-II, demonstrating Q_0 of 2.8×10^{10} at an average accelerating gradient of 16 MV/m in the CW operation of a superconducting linac [3]. The LCLS-II-HE cryomodule with a 2/0 N-doping recipe achieved a maximum acceleration voltage of 208 MV in CW mode, corresponding to an average accelerating gradient of 25.1 MV/m, and Q_0 of 3.0×10^{10} at a gradient of 21 MV/m [21]. Mid-T baking is a novel and simplified high-Q_0 recipe that yields results similar to those of N-doping, while preventing the formation of NbN precipitates, which act as defects, and reducing the risk of contamination. The Institute of High Energy Physics (IHEP) developed the first high-Q_0 cryomodule equipped with eight mid-T-baked cavities, achieving Q_0 of 3.8×10^{10} at 16 MV/m and Q_0 of 3.6×10^{10} at 21 MV/m in horizontal testing [22].

At the Shanghai Advanced Research Institute (SARI), we conduct experimental cavity treatments using facilities for SRF cavity surface treatments on a platform located in Wuxi, China [23]. Both N-doping and mid-T baking recipes have been studied, achieving high accelerating gradients exceeding 25 MV/m on 1.3 GHz 9-cell cavities [24]. Since 2020, several sets of cryomodules with high-Q_0 cavities have been assembled and tested [25]. In this letter, we report the first 1.3 GHz high Q_0 cryomodule dedicated to CW operation up to 1 mA, developed at SARI. It is equipped with eight mid-T-baked cavities and eight 30 kW FPCs [26, 27], demonstrating world-leading, ultra-high Q_0 and ultra-high accelerating gradient performance in CW horizontal testing.

2 Mid-T baked cavities

The eight cavities were mechanically fabricated by the HE-Racing Technology Company in Beijing, treated by the SHINE cavity surface treatment facilities in Wuxi [23], and tested at the SARI and IHEP vertical test (VT) stands. These cavities underwent 200 µm electropolishing, 3 h of 900 °C high-temperature baking, exposure to air, and 3 h of furnace baking at 300 °C [24].

Figure 1 shows the vertical test results of the eight dressed cavities treated with the mid-T-baked recipe, where Q_0 is corrected by the 0.8 nΩ loss of the stainless-steel flanges. The sudden drop of Q_0 at around 16 MV/m for FV007-J, 23 MV/m for FV006-J, and 25 MV/m for GY002-J is attributed to flux trapping after soft quenches caused by multipacting [28], which can be recovered after warming up and performing a fast cooldown. For a direct comparison between the vertical and horizontal tests, the Q_0 drop was compensated for by the gap. The average Q_0 was 4.0×10^{10} at 20 MV/m, and the average maximum gradient was 29.4 MV/m. Three

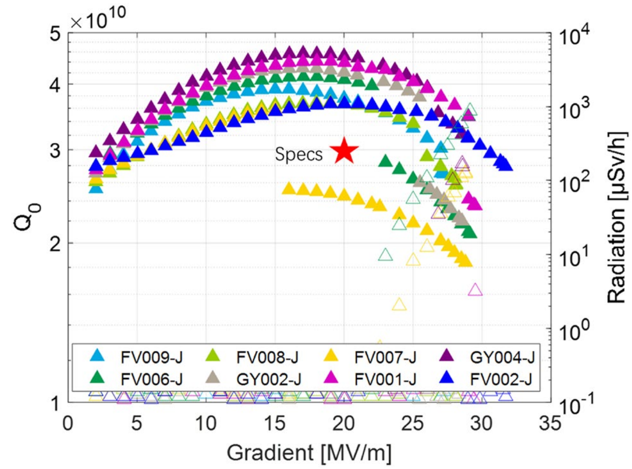

Fig. 1 (Color online) Vertical test results of the eight dressed cavities. The solid triangle represents the Q_0 value, while the hollow triangle represents the radiation dose. The Q_0 values are corrected by 0.8 nΩ loss of stainless-steel flanges. The three cavities with significant radiation dose were cleaned again by high-pressure rinsing before delivery to the cryomodule assembly, without additional vertical testing

cavities exhibiting field emission during the vertical test were cleaned by long, high-pressure rinsing with two rounds of six turns before delivery to the cryomodule assembly. Although no further vertical tests were performed on these three cavities due to the tight schedule, as shown in the horizontal test results, all field emissions were eliminated.

3 Cryomodule assembly

The cryomodule assembly includes clean assembly of the cavity string in a class 10 cleanroom, the cold mass, and the final assembly, typically completed within approximately two months. Before string assembly, all cavities underwent an outer surface rinsing process, after which they entered the cleanroom for more thorough cleaning, including wiping the outer surface, particularly the helium vessel bellows. The surface was blown with clean nitrogen gas to verify contamination levels met class 10 cleanroom standards. The assembly process began with the installation of fundamental power couplers, followed by intercavity bellows from upstream to downstream. Figure 2 shows the cavity-string assembly of the SARI cryomodule (CM) in a class 10 cleanroom.

During assembly, nitrogen gas was vented into the cavities at 1 slm to maintain slightly positive pressure, preventing contamination from entering. Once the string assembly was completed, positive-pressure leak detection was conducted to identify major leaks. The cavity string was then evacuated into a vacuum, followed by a second leak test under vacuum conditions. Residual gas analysis assessed the cleanliness of the entire cavity string. After completing

Fig. 2 (Color online) Cavity-string assembly in class 10 cleanroom

these tests, the cavity string was backfilled with nitrogen to a pressure of 1050 mbar, slightly higher than atmospheric pressure, for protection, and subsequently transported out of the cleanroom for further assembly.

4 Degaussing and cooling down

The cryostat was first degaussed in an east–west direction at SARI. During cryomodule assembly, two flux gates were mounted along the beam direction at the cavity 1# and 5# slots between the two layers of magnetic shields outside the cavity helium vessel. After the cryomodule was installed on the horizontal test stand, the entire cryomodule was degassed at room temperature, as shown in Fig. 3a. The magnetic field falls from 2.6 mGs to 0.3 mGs and from 0.9 to 0.7 mGs after degaussing for the cavities 1# and 5#, respectively, as shown in Fig. 3b.

The SARI cryomodule cooling process, from 300 K to 2 K, follows a procedure similar to that of the European XFEL [29] and LCLS-II [30], typically lasting for 3~4 days. From 300 K to 45 K, the average cooling rate has been controlled at around 6 K/h, followed by a "stand-by mode" lasting for about 12 h to allow the entire cryomodule cold mass to stabilize at the 45 K temperature level. Fast cooling from 45 K to 4.5 K is required for magnetic flux exclusion in high-Q cavities, improving RF performance [31]. Once liquid helium accumulates along the cavity string and in the two-phase pipe, most of the cold mass is cooled to approximately 4.5 K. Final cooling is achieved by depressurizing the saturated helium vapor from around 1.2 to 31 mbar, reaching the operating condition at 2 K superfluid helium. Figure 4 shows the first cooling step of the standard SARI cryomodule.

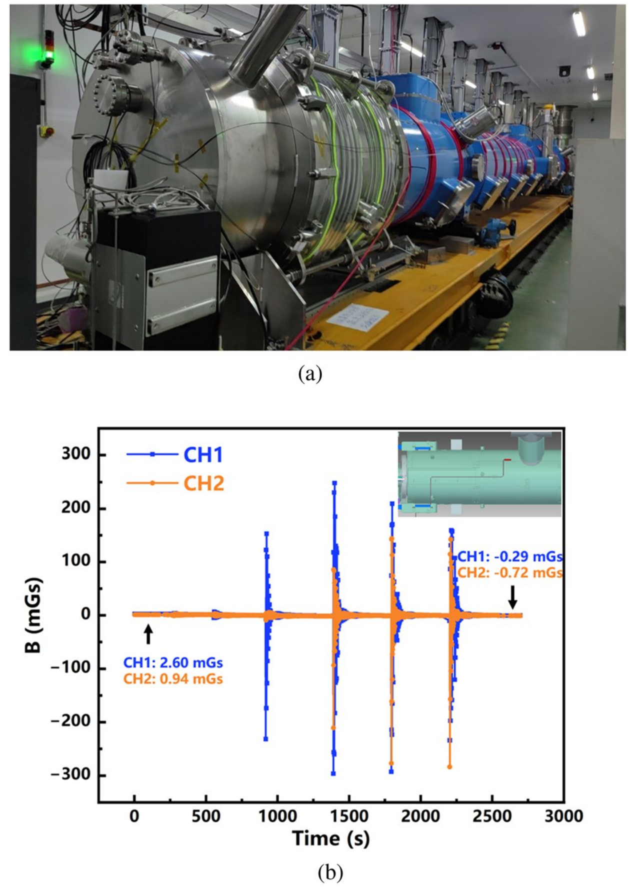

Fig. 3 (Color online) (a) The coils wound for cryomodule degaussing in the horizontal test stand; (b) In-situ cryomodule degaussing at room temperature before cooling down. The two flux gates are mounted at cavity 1# and 5# slots, between the two layers of magnetic shields outside the cavity helium vessel, as shown in the upper-right inset image

A key method to achieve high Q_0 performance at 2 K is to maintain an instant liquid-helium mass flow rate, creating a sufficient thermal gradient for magnetic flux expulsion as the cavities pass through the superconducting transition point (T_c) of approximately 9.2 K [31, 32]. Before the Q_0 test, the cryomodule was warmed up to 45 K and then quickly cooled again to release the magnetic flux trapped during previous quenches, which reached their maximum gradient or were induced by multipacting. For the SARI cryomodule, a maximum flow rate of 41.6 g/s was achieved when the cavities passed through the T_c. Figure 5 shows the thermal difference between the top and bottom of the dressed cavities during the horizontal test, where thermal sensors are mounted outside dressed cavities 1#, 5# and 8#.

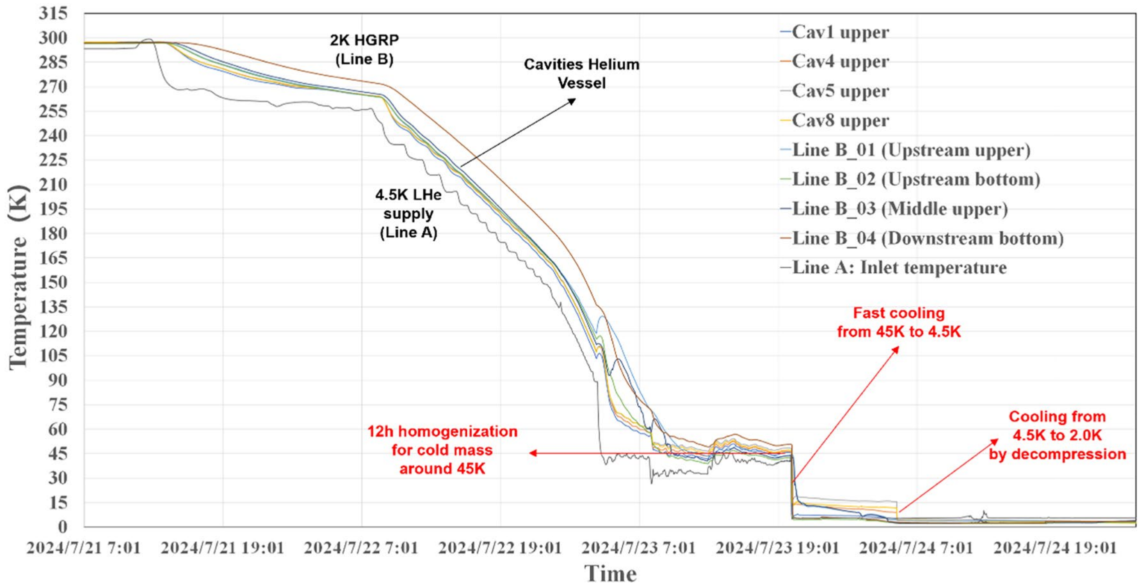

Fig. 4 (Color online) Cooling curves of the SARI cryomodule from 300 K to 2 K

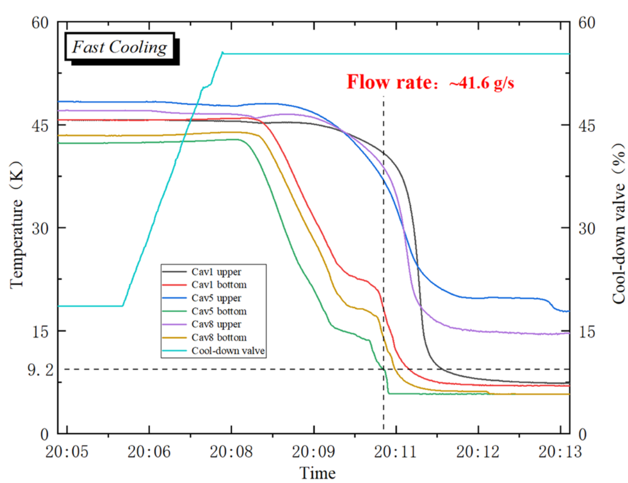

Fig. 5 (Color online) Fast cooling curves for SARI cryomodule from 45 K to 4.5K

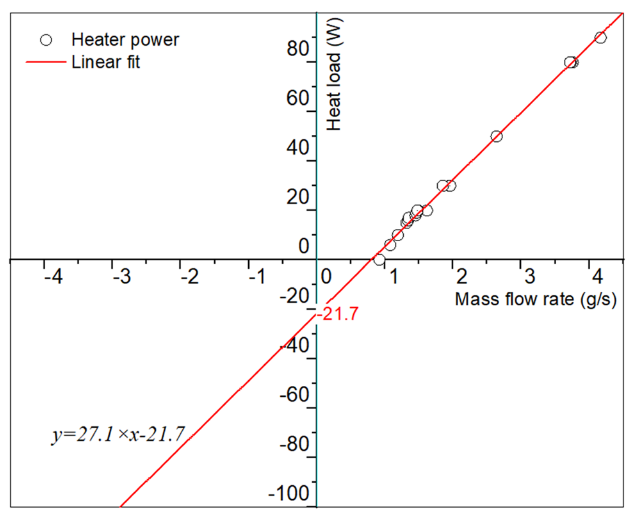

Fig. 6 (Color online) Static heat load measurements for the SARI cryomodule at 2 K: the overlap of circles at 20, 30, and 80 W serves to verify the data's repeatability and reliability

5 Q_0 performance

The mass flow rate method was employed to measure the static and dynamic 2 K heat load of the cryomodule [33–35]. Figure 6 shows the calibration results of the heat load via heaters for the SARI CM. The CM was first injected with liquid helium above half of the two-phase pipe and then evaporated in a semi-closed system (i.e., a cavity string with supply valves closed and the helium-gas-return pipe valve opened) under different heat load conditions ranging from 0 to 90 W. According to the law of conservation of energy, when dynamic balance is achieved, the helium evaporating mass flow rate, along with its latent heat (~23 J/g at 2 K) takes the same energy deposited on the 2 K cold mass from the outside heat load. With the above relationship between heat load and evaporating mass flow rate, a linear fit can be obtained based on the thermal heater power and flowmeter measurements. Consequently, the absolute value of the intercept point at "zero" mass flow rate gives the 2 K static heat load of the SARI cryomodule around 21.7 W, as shown in Fig. 6.

The dynamic heat load of each cavity was measured by subtracting the heat load of three cavities from four cavities to improve accuracy. The estimated measurement uncertainty of Q_0 was less than 10%, and the accelerating gradient was less than 5%.

To directly compare Q_0 between vertical and horizontal tests, Q_0 values with a sudden drop in three cavities were compensated for by the gap at the drop gradient. Figure 7 shows a comparison of Q_0 at 20 MV/m for the eight dressed cavities in both vertical and horizontal tests.

The average Q_0 values at 166 MV and higher voltages in CW mode were also measured for the SARI CM. The total 2 K heat load was 104.9 W at a total voltage of 166.1 MV with all eight cavities at 20 MV/m, 194.9 W at 223.8 MV, and 236.4 W at 241.3 MV, corresponding to an average Q_0 of 4.0×10^{10} at a gradient of 20 MV/m, 3.4×10^{10} at 27 MV/m, and 3.2×10^{10} at 29 MV/m, respectively. Figure 8 provides the measurement points of the SARI CM and compares them with other top cryomodules [9, 21, 22].

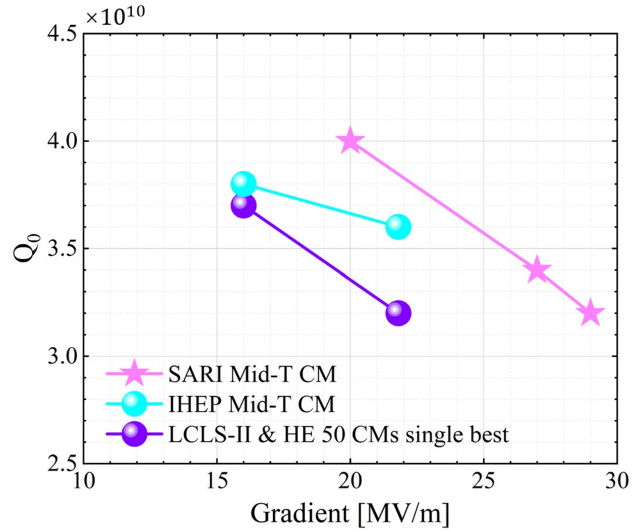

Fig. 8 (Color online) Average Q_0 at 20, 27, and 29 MV/m for the SARI cryomodule in the horizontal test, compared with other top-performing cryomodules [21, 22] in the world. The administration limit for LCLS-II HE cryomodule testing is 26 MV/m for each cavity, corresponding to a maximum CM voltage of 216 MV [9]

6 Gradient performance

Figure 9 shows the maximum accelerating gradients for the eight dressed cavities measured in CW mode during vertical tests and in the cryomodule, where the maximum gradient is defined as stable operation for at least one minute. The usable gradient in the cryomodule is defined as meeting the conditions of being 0.5 MV/m less than the quench field, stable operation for one hour, and radiation dose less than 500 µSv/h measured by the G-M tube radiation detectors placed around 2 m from the cryomodule in the horizontal test stand. As can be seen, all cavities approach full-gradient performance except for cavity 5#, which is limited by HOM heating, as described below.

To accelerate a beam, long-term stable operation at the working gradient is essential for the CM. During operation, RF power can heat the FPC antennas, which are cooled through a ceramic window and CF100 flange by a 45 K intercept, a conduction-cooling braid connected to the 45 K helium gas pipes, eventually reaching thermal equilibrium. For the SARI CM, the temperature of each CF100 flange was monitored using thermal sensors. A stable operation test was performed at 220 MV for the SARI CM. The external

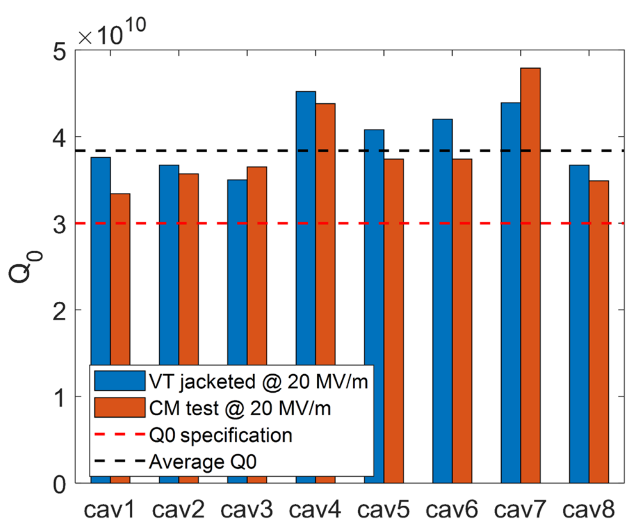

Fig. 7 (Color online) Q_0 measured at 20 MV/m for each cavity in both vertical and horizontal tests. To allow direct comparison, the Q_0 values of cavities 3#, 5#, and 6# were adjusted to account for the Q_0 gap in vertical tests due to flux trapping after soft quenches

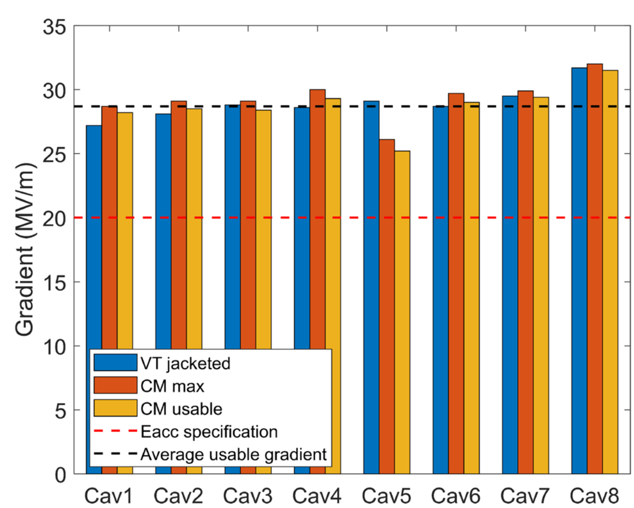

Fig. 9 (Color online) Accelerating gradient measured for each jacketed-cavity in vertical and horizontal tests

Q values of the eight cavities were adjusted to their optimal values of approximately 6.1×10^7 for a working gradient of 20 MV/m. Due to the cryogenic limit of the horizontal test stand, the eight cavities were split into two groups for stable operation testing. Each cavity operated at 27.3 MV/m, except for cavity 5# at 21.7 MV/m. The group with the first four cavities maintained a total voltage of 113 MV, while the other group maintained 108 MV. To reduce test time, we detuned the phase of the self-excited loop to increase reflected power, thus heating the main coupler to its threshold of approximately 150 K. Afterward, we tuned it back and awaited thermal equilibrium, or maintained it for 10 h. Figure 10 shows the temperature behavior of the eight FPC CF100 flanges during the 220 MV stable operation test. As shown, all the temperatures of the eight CF100 flanges decreased, reaching quasi-equilibrium, with a maximum temperature of less than 120 K, below the 150 K threshold. This confirms the stable operation capacity at 220 MV for this CM.

Table 1 summarizes the CW mode performances of the eight mid-T-baked cavities in VT and CM. The Q_0 of the entire CM measurement was 4.0×10^{10} at 166 MV, with all eight cavities operating simultaneously at 20 MV/m. The slight difference in the average Q_0 between the individual cavities and the entire CM measurement was likely due to the uncertainty of the small heat load, as shown in Fig. 6.

It is worth mentioning that the cryomodule was also tested in pulsed mode with a repetition rate of 0.5 Hz and a 10% duty factor, where the total accelerating voltage reached 247.6 MV. In this mode, cavity 5# was powered up to 29.2 MV/m, the same as its maximum gradient in the vertical test. Additionally, no detectable field emissions were observed during any of the cryomodule tests.

7 Limitation factor

When comparing the RF performances of the eight cavities in the vertical and horizontal tests, cavity 5# exhibited a significant decrease in the accelerating gradient. The maximum CW operating gradient for cavity 5# was limited to approximately 25.2 MV/m by quenching, accompanied by a rapid temperature increase at the FPC-side HOM coupler, where the thermal sensor was mounted on the copper clamp at the copper sleeve of the HOM-feedthrough, as shown in Fig. 11.

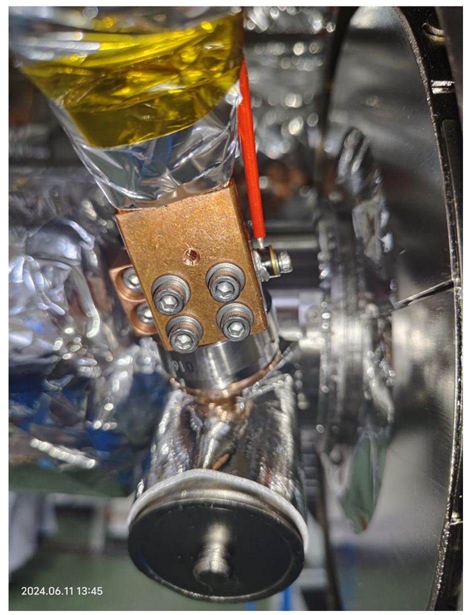

Fig. 11 (Color online) A thermal sensor is mounted on the conducted-cooling clamp of a HOM-feedthrough copper sleeve at the cavity 5# FPC-side to monitor HOM heating

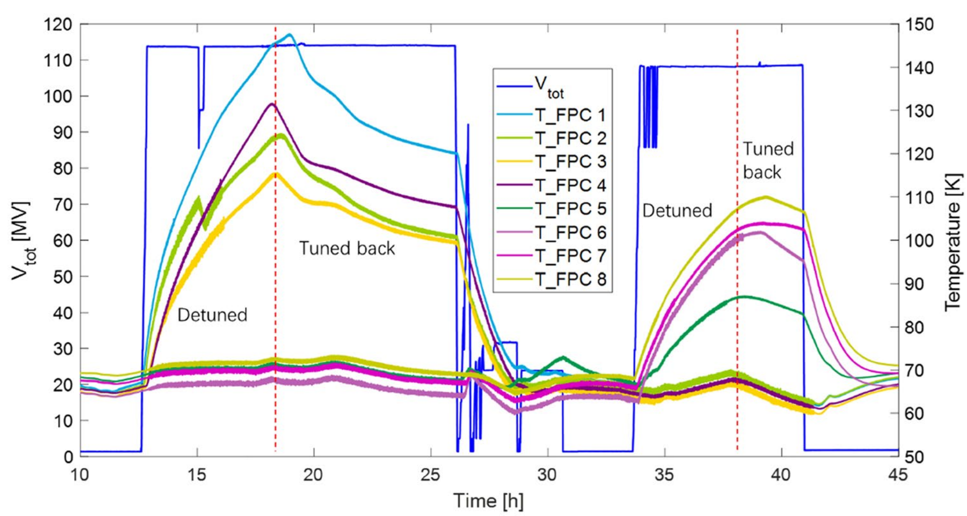

Fig. 10 (Color online) Long-term stable operation test at 220 MV for SARI CM, monitoring the temperature of the FPC CF100 flanges connected to the 45 K intercept. The test was performed in two groups, with four cavities each. The phases of the self-excited loop were detuned to speed up the FPC heating to a maximum of around 150 K for FPC1, then tuned back, as shown by the turning points marked by the red dashed lines

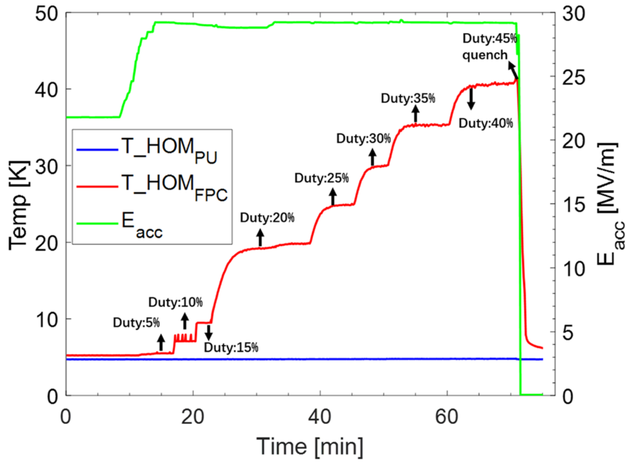

Fig. 12 (Color online) Accelerating gradient of cavity 5# limited by FPC-side HOM heating, where the thermal sensors are mounted on the copper sleeve of HOM-feedthroughs

To investigate the limiting factor, we tested cavity 5# in pulsed mode. With a repetition rate of 0.5 Hz and a duty cycle of 5%, we began increasing the input power to the cavity, which showed that the cavity could stably operate at 29.2 MV/m, similar to the maximum gradient in the vertical test, with a slight temperature increase at the FPC-side HOM. We then gradually increased the duty cycle in steps of 5%, while maintaining a gradient of 29.2 MV/m, and a positive correlation between the FPC-side HOM temperature and duty cycle was observed. The cavity could stably operate at 29.2 MV/m with a duty cycle of up to 40%, where the HOM temperature approached approximately 40 °C, but quenched quickly once the duty cycle was increased to 45%. Figure 12 shows the relationship between the HOM temperature and the duty cycle for cavity 5#. It is important to note that no field emissions were observed during these measurements. Therefore, we concluded that the limitation of cavity 5# gradient is due to overheating of the HOM antenna.

8 Conclusion

A high Q_0 cryomodule equipped with eight mid-T-baked 1.3 GHz 9-cell cavities was assembled and tested at SARI. This cryomodule achieved an ultra-high average Q_0 at the operating gradients and an unprecedented total accelerating voltage in CW mode. The cryomodule's average Q_0 was 4.0×10^{10} at 20 MV/m and 3.2×10^{10} at 29 MV/m in the horizontal test, which corresponds to a maximum CW RF voltage of approximately 241 MV. The RF performance of the cavities was well-maintained from the vertical test to the horizontal test. Furthermore, no field emissions were observed in any of the eight cavities in the cryomodule. The successful development of this ultra-high Q_0 and ultra-high gradient cryomodule demonstrates the techniques mastered from components to a completed cryomodule, marking an important milestone for CW accelerator projects, such as high-repetition X-ray FEL facilities, high-power extreme ultraviolet lithography light sources, and other future high-duty factor colliders.

Table 1 Summary of individual cavity performance in the VT and cryomodule. The VT Q_0 values are corrected for stainless-steel flange losses (0.8 nΩ subtracted). "*"indicates that the Q_0 was compensated for by the drop in Q_0 during the vertical test owing to flux trapping after soft quenching

Slot in CM	SN	Vertical test E_{max} (MV/m)	Vertical test $Q_0/10^{10}$ at 20 MV/m	Cryomodule test E_{max} (MV/m)	Cryomodule test E_{usable} (MV/m)	Cryomodule test FE onset (MV/m)	Cryomodule test $Q_0/10^{10}$ at 20 MV/m
1	FV009-J	27.2	3.8	28.7	28.2	None	3.3
2	FV008-J	28.1	3.7	29.1	28.5	None	3.6
3	FV007-J	28.8	3.5*	29.1	28.4	None	3.7
4	GY004-J	28.6	4.5	30.0	29.3	None	4.4
5	FV006-J	29.1	4.1*	26.1	25.2	None	3.7
6	GY002-J	28.7	4.2*	29.7	29.0	None	3.7
7	FV001-J	29.5	4.4	29.9	29.4	None	4.8
8	FV002-J	31.7	3.7	32.0	31.5	None	3.5
Average		29.0	4.0	29.3	28.7		3.8

Acknowledgements The authors would like to thank all the colleagues who contributed to this work, including the SRF cryomodule, cryogenic, and general technology teams, as well as the companies and institutes that supplied the cryomodule components and technical servers. The authors are grateful to Mi-Yi-Min Zhao and Xing-Heng Wang for the helps in figure drawing.

Author Contributions All authors contributed to and participated in the design, manufacturing, assembly, and testing of the cryomodule. Jin-Fang Chen was the cryomodule coordinator. Hai-Xiao Deng was the project leader. The first draft of the manuscript was written by Jin-Fang Chen, Meng Zhang, Hai-Xiao Deng, and all authors commented and reviewed on previous versions and the final version of the manuscript.

Data Availability The data that support the findings of this study are openly available in Science Data Bank at https://cstr.cn/31253.11.sciencedb.j00186.00460 and https://www.doi.org/10.57760/sciencedb.j00186.00460.

Declarations

Conflict of interest Hai-Xiao Deng and Zhen-Tang Zhao are editorial board members for Nuclear Science and Techniques and were not involved in the editorial review, or the decision to publish this article. All authors declare that there are no conflict of interest.

References

1. N. Huang, H. Deng, B. Liu et al., Features and futures of X-ray free-electron lasers. Innovation **2**, 100097 (2021). https://doi.org/10.1016/j.xinn.2021.100097
2. N. Nakamura, R. Kato, H. Sakai et al., High-power EUV free-electron laser for future lithography. J. Appl. Phys. **62**, SG0809 (2023). https://doi.org/10.35848/1347-4065/acc18c
3. J. Gao, CEPC technical design report: accelerator. Radiat. Detect. Technol. Methods **8**, 1–1105 (2024). https://doi.org/10.1007/s41605-024-00463-y
4. N. Huang, Z. Liu, B. Deng et al., The MING proposal at SHINE: megahertz cavity enhanced X-ray generation. Nucl. Sci. Tech. **34**, 6 (2023). https://doi.org/10.1007/s41365-022-01151-6
5. B. Aune, R. Bandelmann, D. Bloess et al., Superconducting TESLA cavities. Phys. Rev. ST Accel. Beams **3**, 092001 (2000). https://doi.org/10.1103/PhysRevSTAB.3.092001
6. C. Pagani, J. Weisend II., R. Bandelmann et al., construction, commissioning, and cryogenic performances of the first TESLA test facility (TTF) cryomodule. Adv. Cryogenic Eng. (1998). https://doi.org/10.1007/978-1-4757-9047-4_9
7. C. Madec, S. Berry, P. Charon et al., Status of E-XFEL String and Cryomodule Assembly at CEA-Saclay. in Proceedings of LINAC2012, Tel-Aviv, Israel (2012)
8. T. Arkan, C. Ginsburg, Y. He et al., LCLS-II 1.3 GHz Design integration for assembly and cryomodule assembly facility readiness at Fermilab. In: Proceed. SRF2015, Whistler, BC, (2015)
9. J. Maniscalco, *LCLS-II-HE cavity and cryomodule test progress* (IL, TESLA Technology Collaboration (TTC) Meeting, Fermilab, Batavia, (2023)
10. A. Grassellino, A. Romanenko, D. Sergatskov et al., Nitrogen and argon doping of niobium for superconducting radio frequency cavities: a pathway to highly efficient accelerating structures. Supercond. Sci. Technol. **26**, 102001 (2013). https://doi.org/10.1088/0953-2048/26/10/102001
11. A. Palczewski, Analysis of Bcs Rf loss dependence on N-doping protocols. In: Proceed. SRF2015, Whistler, BC (2015)
12. D. Bafia, Optimization of high temperature nitrogen doping TESLA technology collaboration (TTC) Meeting. Milano, Italy (2018)
13. Y. Zong, J. Chen, D. Wang et al., Accelerating gradient improvement in nitrogen-doped superconducting radio-frequency cavities for SHINE. Nucl. Instrum. Methods Phys. Res. Sec. A **1057**, 168724 (2023). https://doi.org/10.1016/j.nima.2023.168724
14. P. Dhakal, Nitrogen doping and infusion in SRF cavities: a review. Phys. Open **5**, 100034 (2020). https://doi.org/10.1016/j.physo.2020.100034
15. S. Posen, A. Romanenko, A. Grassellino et al., Ultra-low surface resistance via vacuum heat treatment of superconducting radiofrequency cavities. Phys. Rev. Appl. **13**, 014024 (2019). https://doi.org/10.1103/PhysRevApplied.13.014024
16. H. Ito, H. Araki, K. Takahashi et al., Influence of furnace baking on Q-E behavior of superconducting accelerating cavities. Prog. Theor. Exp. Phys. **2021**, 071G01 (2021). https://doi.org/10.1093/ptep/ptab056
17. F. He, W. Pan, P. Sha et al., Medium-temperature furnace baking of 1.3 GHz 9-cell superconducting cavities at IHEP. Supercond. Sci. Technol. **34**, 095005 (2021). https://doi.org/10.1088/1361-6668/ac1657
18. H. Padamsee, Superconducting radiofrequency technology for accelerators - state of the art and emerging trends (WILEY-VCH GmbH) (2023), p. 45
19. G. Wu, A. Grassellino, E. Harms et al., Achievement of Ultra-High Quality Factor in Prototype Cryomodule for LCLS-II. arXiv:1812.09368, (2018)
20. R. Legg, G. Cheng, E. Daly et al., LCLS-II Cryomodule Production at JLab. In: Proceed. SRF2017, Lanzhou, China (2018)
21. S. Posen, A. Cravatta, M. Checchin et al., High gradient performance and quench behavior of a verification cryomodule for a high energy continuous wave linear accelerator. Phys. Rev. Accel. Beams **25**, 042001 (2022). https://doi.org/10.1103/PhysRevAccelBeams.25.042001
22. W. Pan, J. Zhai, F. He et al., High Q and high gradient performance of first medium-temperature baking 1.3 GHz cryomodule. Phys. Rev. Accel. Beams **27**, 092003 (2024). https://doi.org/10.1103/PhysRevAccelBeams.27.092003
23. J. Chen, S. Xing, J. Wu et al., Design, construction and operation of a surface-treatment platform for SHINE superconducting cavities. In: Proceed. IPAC'24, Nashville, TN, USA (2024)
24. Y. Zong, Q. Chen, X. Huang et al., Realization of accelerating gradient larger than 25 MVm on high-Q 1.3 GHz 9-cell cavities for SHINE. In: Proceed. SRF2023, Grand Rapids, MI, USA (2023)
25. J. Chen, H. Hou, Z. Ma et al., Cryomodules development for SHINE project. In: Proceed. IPAC'24, Nashville, TN, USA (2024)
26. Z. Ma, Lessons learned on coupler fabrication for SHINE. TTC2024 Meeting, ESS Lund, Sweden (2024)
27. Z. Ma, H. Hou, S. Zhao et al., Manufacturing studies and rf test results of the 1.3 GHz fundamental power coupler prototypes. Phys. Rev. Accel. Beams **25**, 113501 (2022). https://doi.org/10.1103/PhysRevAccelBeams.25.113501
28. D. Bafia, A. Grassellino, A. Romanenko et al., New Insights on Nitrogen Doping. In: Proceedings of SRF2019, Dresden, Germany (2019)
29. A. Navitski, Cavities/modules test facility AMTF at DESY. Americas Workshop on Linear Colliders 2014, Fermilab (2014)
30. G. Wu, E. Harms, A. Grassellino et al., Performance of the high Q CW prototype cryomodule for LCLS-II at FNAL. In: Proceed. SRF2017, Lanzhou, China (2017)
31. S. Posen, G. Wu, A. Grassellino et al., Role of magnetic flux expulsion to reach Q_0>3×10^{10} in superconducting rf cryomodules. Phys. Rev. Accel. Beams **22**, 032001 (2019). https://doi.org/10.1103/PhysRevAccelBeams.22.032001

32. D. Gonnella, R. Eichhorn, F. Furuta et al., Nitrogen-doped 9-cell cavity performance in a test cryomodule for LCLS-II. J. Appl. Phys. **117**, 023908 (2015). https://doi.org/10.1063/1.4905681
33. X. Wang, S. Barbanotti, J. Eschke et al., Thermal performance analysis and measurements of the prototype cryomodules of European XFEL accelerator-Part II. Nucl. Instrum. Methods Phys. Res. Sec. A **763**, 688–700 (2014). https://doi.org/10.1016/j.nima.2014.07.045
34. E. Harms, LCLS-II cryomodule heat load measurements at Fermilab. TESLA Technology Collaboration (TTC) Meeting (2021)
35. W. Pan, R. Ge, M. Li et al., Cryogenic system of the high performance 1.3 GHz 9-cell superconducting radio frequency prototype cryomodule. Appl. Thermal Eng. **255**, 124042 (2024). https://doi.org/10.1016/j.applthermaleng.2024.124042